J Mater Sci (2018) 53:385–395

Chemical routes to materials

3D hierarchical flower-like rutile TiO_2 nanospheres-based versatile photocatalyst

Yibo Du[1], Xiaoyu Xu[1], Lin Lin[2,*], Meiying Ge[2], and Dannong He[1,2,*]

[1] School of Materials Science and Engineering, Shanghai Jiao Tong University, Shanghai 200240, China
[2] National Engineering Research Center for Nanotechnology, Shanghai 200241, China

Received: 29 March 2017
Accepted: 22 August 2017
Published online: 29 August 2017

ABSTRACT

3D hierarchical flower-like TiO_2 nanospheres with rutile phase were synthesized via a facile hydrothermal method without further calcination. The morphology, crystalline phase and pore structure of the products were characterized by scanning electron microscope, transmission electron microscope, X-ray diffraction, Raman and nitrogen adsorption–desorption test. The results show that the hierarchical flower-like TiO_2 nanospheres are assembled from well-ordered nanorods. It is found that the nanostructure of TiO_2 nanospheres varies with the elevation of reaction temperatures, indicating a critical effect on the formation of hierarchical TiO_2 nanospheres with a large proportion of (110) facets. The obtained TiO_2 nanospheres can be used as photocatalyst, and the photocatalytic activity was evaluated by photodegrading a complex dye solution containing rhodamine B and methylene blue. It turned out that the TiO_2 photocatalysts prepared at 160 and 190 °C showed the highest photocatalytic activity under ultraviolet light irradiation.

Introduction

Since the pioneering work about photosplitting of water on TiO_2 electrode reported by Honda and Fujushima [1], photocatalysts have become the ideal solution to eliminate dye pollutants. Among the various semiconductor metal oxides, TiO_2 has been always regarded as one of the most promising photocatalysts due to its high chemical stability and activity, non-toxicity, corrosion resistance and low cost [2–4]. But, there is still a problem that TiO_2 can only catalyze simple dye. In order to expand photodegrading scale, this material needs to be doped and modified [5–8]. To the best of our knowledge, there is a little report on photodegrading a complex dye solution. As a result, the development of photocatalyst that can degrade complex dyes simultaneously with high efficiency has received great attention.

As is well known, the photocatalytic performance of TiO_2 strongly depends on its morphology, structure, size, crystal phase and surface property [9, 10]. Up to now, many kinds of TiO_2 morphologies have been synthesized, such as nanoparticles, naonorods, nanosheets [11–13] and so on. Among various

Address correspondence to E-mail: linlin21023@163.com; hdn_nercn@163.com

DOI 10.1007/s10853-017-1498-3

morphologies, hierarchical 3D architecture has attracted extensive attention because they may exhibit interesting properties due to the large numbers of active sites, unique multidimensional morphology and the combination of micro–nanoscales [14–19]. Therefore, 3D architecture self-assembled by 1D nanostructure is very essential, and there are few reports on this kind of nanocomposite for photocatalysts.

To date, the majority of studies of TiO_2 photocatalysts have focused on anatase phase. There seems to be a general agreement that the anatase crystal structure exhibits higher photocatalytic activities than rutile [20–22], but through the change in the structure and surface area, the rutile phase photocatalysts can also works well. Some researchers have pointed out that the poor catalytic activity of rutile structured powders may be related with the low surface area and the poorly controlled morphology [23], rutile TiO_2 can also be prepared with high specific surface area [24–26]. There are also some reports mentioned that the rutile crystalline have the same photoactivity as anatase, or even higher [27–29], which may be a comprehensive result of multifactors, such as specific surface area, pore size distribution, crystal size and so on. More importantly, the Fermi level in rutile is lower than that of anatase by about 0.1 eV, indicating that rutile TiO_2 should be more suitable for practical application. However, studies of hierarchical TiO_2 nanostructures with rutile phase applied in photocatalysts are far from satisfactory [30, 31].

In this research, we fabricate a novel self-assembly 3D hierarchical flower-like rutile TiO_2 successfully through hydrothermal method without further calcination, and the formation mechanism is also speculated. The photocatalytic performance of the hierarchical TiO_2 nanospheres is investigated by photodegrading a complex dye solution containing methylene blue (MB) and rhodamine B (RhB) simultaneously [32, 33]. Moreover, the photocatalysis kinetics of the rutile TiO_2 nanospheres is also evaluated.

Experimental

Reagents and materials

All chemicals used in this study were analytical-grade reagents. Titanium (IV) butoxide ($Ti(OC_4H_9)_4$, TBOT), hydrochloric acid (HCl, 37 wt%), nitric acid (HNO_3), sulfuric acid (H_2SO_4), phosphoric acid (H_3PO_4) and glacial acetic acid (CH_3COOH) were purchased from Shanghai Chemical Co. China. Methylene blue (MB) and rhodamine B (RhB) were purchased from Shanghai Chemical Co. China, which were used as the target dye for photodegradation experiments. Deionized water was used for all experiments.

Preparation of 3D hierarchical flower-like TiO_2 photocatalysts

In a typical procedure, 15 ml of hydrochloric acid (HCl, 37 wt%) and 15 ml of deionized water were mixed in equal volume with a total volume of 30.0 ml. Then, 3.0 ml of TBOT was dissolved in the solution by magnetic stirring. After stirring for 1 h, the homogeneous solution was transferred to a 45-ml Teflon-lined stainless steel autoclave followed by heating at different temperatures from 160 to 190 °C for 3 h. Finally, the synthesized products were thoroughly washed with deionized water and dried at 80 °C in air for 12 h. The samples synthesized at 160, 170, 180, 190 °C were marked as S_{160}, S_{170}, S_{180}, and S_{190}, respectively.

Photocatalytic activity measurements

The photodegradation reactions were carried out under atmospheric condition using a 300-W mercury lamp as the irradiation source at ambient temperature. The irradiation distance between lamp and sample was 10 cm. Hundred milligrams of TiO_2 photocatalysts was added into a cylindrical glass vessel containing 100 ml of complex solution with a concentration of 10 mg/l RhB and 10 mg/l MB, respectively. Before exposing the samples to the light source, the solution was agitated thoroughly with the catalyst slide in the dark for 30 min to reach the adsorption equilibrium of the dye on the catalyst. At intervals, the photodegradation reaction was ceased and the solution was centrifuged. The residual dye concentration in the supernatant was measured by a

UV–Vis spectrometer (Lambda 850) at maximum absorption wavelength. Parallel degradation reactions under same conditions were conducted for varied time intervals. The intensity of the absorption band peak was recorded against time.

Characterization methods

The morphologies and nanostructures of the samples were investigated by scanning electron microscopy (SEM) using Hitachi S-4800. Transmission electron micrographs (TEM) were taken with JEM-2010F of JEOL electron microscope. X-ray diffraction (XRD) patterns were measured using a D/max-2600PC with Cu Kα radiation ($\lambda = 1.5406$ Å) operated at 40 kV and 150 mA at a scan rate of 5.0°/min. Qualitative analysis was performed with the X'pert High-Score software and the JCPDSPDF-2 database. The average crystallite size was calculated from the Scherrer equation, using the X-ray diffraction peak at $2\theta = 27.4°$ (rutile). Fourier-transformed Raman spectroscopic measurements in the ultraviolet light were taken on a Renishaw inVia Reflex Raman Spectrometer. Nitrogen adsorption–desorption isotherms were measured with Micromeritics ASAP 2010 nitrogen adsorption apparatus. All the samples were degassed at 473 K prior to the measurements. The optical absorption spectra were recorded on a UV–Vis spectrophotometer (Agilent 8453) at room temperature. The Brunauer–Emmett–Teller (BET) method was used for surface area calculation, and the pore size distribution (pore diameter and pore volume of the samples) was determined by the Barrett–Joyner–Halenda (BJH) method.

Results and discussion

Morphology observation

The SEM morphologies of the as-obtained TiO_2 nanoparticles synthesized at different reaction temperatures are shown in Fig. 1. When the temperature was 160 °C, it is found the sample exhibits flower-like nanoclusters with big gaps (Fig. 1a), which are core-centered and radiate outward, and the diameter of each nanocluster is about 4–6 μm. The highly magnified image clearly displays that the samples are composed of numerous well-ordered nanorods with a diameter of about 20 nm (Fig. 1b). The nanorod with tetragonal crystal structure has the trend to aggregate and form a cluster. When the temperature increased to 170 °C (Fig. 1c, d), the intervals narrowed down. The compact architecture has a diameter of 5 μm and a uniform distribution. The highly magnified image demonstrates clearly that these nanorods contain bunch of aligned nanoparticles. Figure 1e shows the morphology of sample fabricated at 180 °C, the gap vanished and formed TiO_2 microspheres with a diameter of 7.5 μm, and the highly magnified image shows that TiO_2 microspheres are composed of uniform distribution nanorods containing bunch of aligned nanoparticles (Fig. 1f). As the temperature continued increasing to 190 °C (Fig. 1g), TiO_2 microspheres with novel hollow urchin nanostructures with 1 mm diameter appeared. However, there was a sunken area at the outer surface of the ball, which promotes the expansion in the specific area and the number of active sites. The 3D dendritic hollow urchin structure may be formed due to selected surface etching of Ti species in strong acid medium at relatively higher temperature.

Figure 2a, d shows representative TEM images of S_{160} and S_{190}, indicating the formation of hierarchical structured TiO_2 composed of nanorods (Fig. 2b, e). High-resolution TEM (HRTEM) analysis was employed to determine the crystal facets. There is no lattice distortion, and all atoms are well aligned in the lattice of the sample S_{160}. The lattice spacing of (110) atomic plane is around 0.32 nm, corresponding to rutile (110) facet. Correspondingly, the digital diffraction pattern (Fig. 2c, inset) displays clear diffraction spots instead of diffraction rings, suggesting a single-crystal-like nature within the whole nanostructure. Moreover, two sets of clear lattice fringe are present in sample S_{190}, indicating their well crystalline structure.

Structural analysis

XRD patterns of the prepared samples demonstrate that the diffraction peaks of samples synthesized at 160, 170 and 180 °C are indexed to pure rutile phase. The main peaks located at approximately 27.5°, 36.1°, 41.3°, 44.1°, 54.4°, 56.7°, 62.8°, 64.1°, 69.1° are observed, which can be readily indexed as the (110), (101), (111), (211), (210), (220), (002), (310), (301) lattice planes of rutile. But when the reaction temperature is 190 °C, small amounts of brookite phase are observed, indicating the formation of biphasial

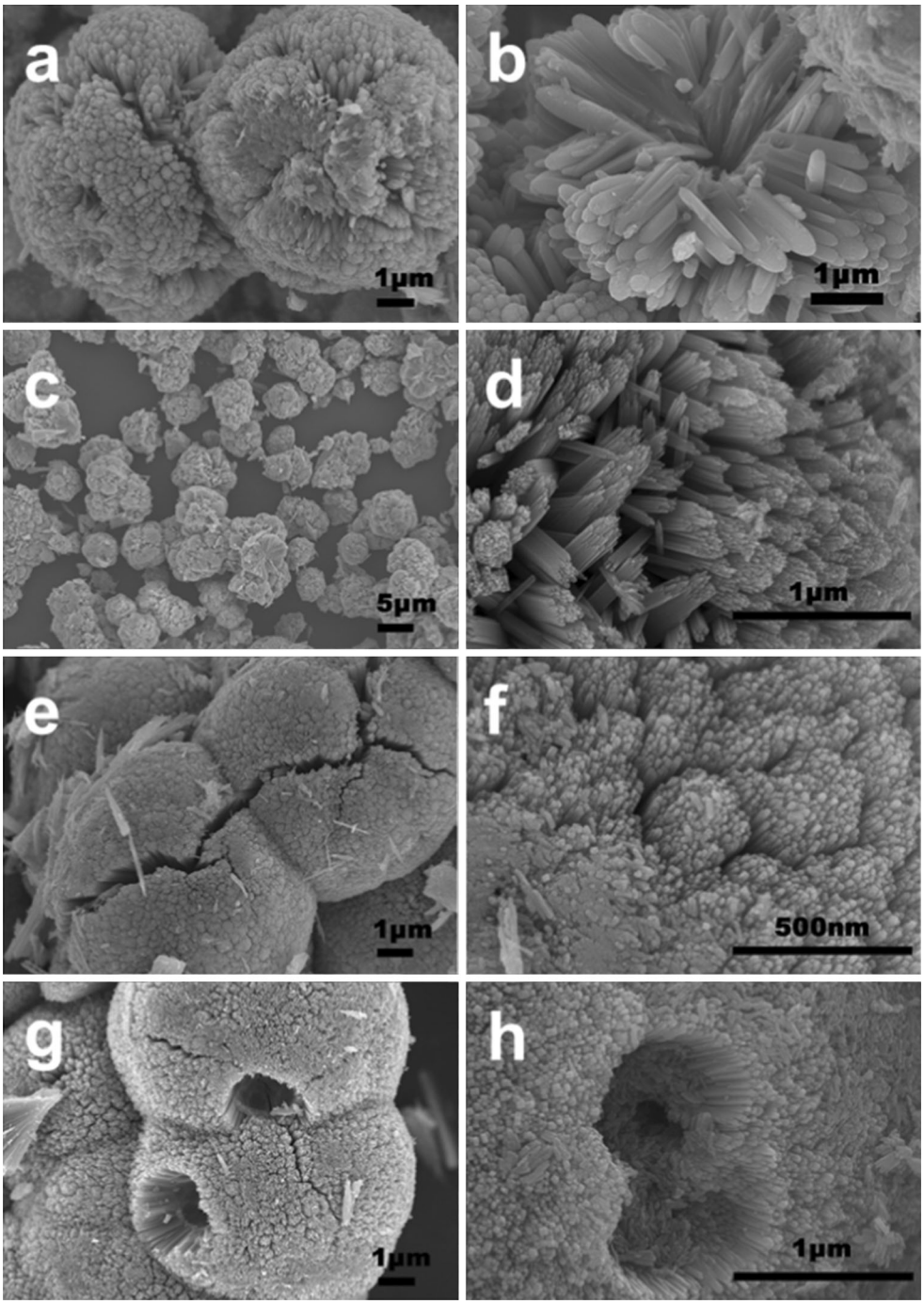

Figure 1 SEM images of hierarchical TiO_2 nanostructures synthesized at: **a**, **b** 160 °C; **c**, **d** 170 °C; **e**, **f** 180 °C; **g**, **h** 190 °C.

rutile/brookite composites. It is speculated that the formation of rutile phase is partly related with the high acidity. When H^+ concentration is higher, it can attack the atom bridge between Ti atoms, break the oxolation bonds and form new species. The new formed species are unstable and lead to structure rearrangement, forming the rutile phase with corner-shared bonding [34].

The crystalline size of the formed TiO_2 was further calculated based on the strongest peak of the XRD patterns via the Scherrer equation (shown in Fig. 3):

$$D = k\lambda/\beta\cos\theta$$

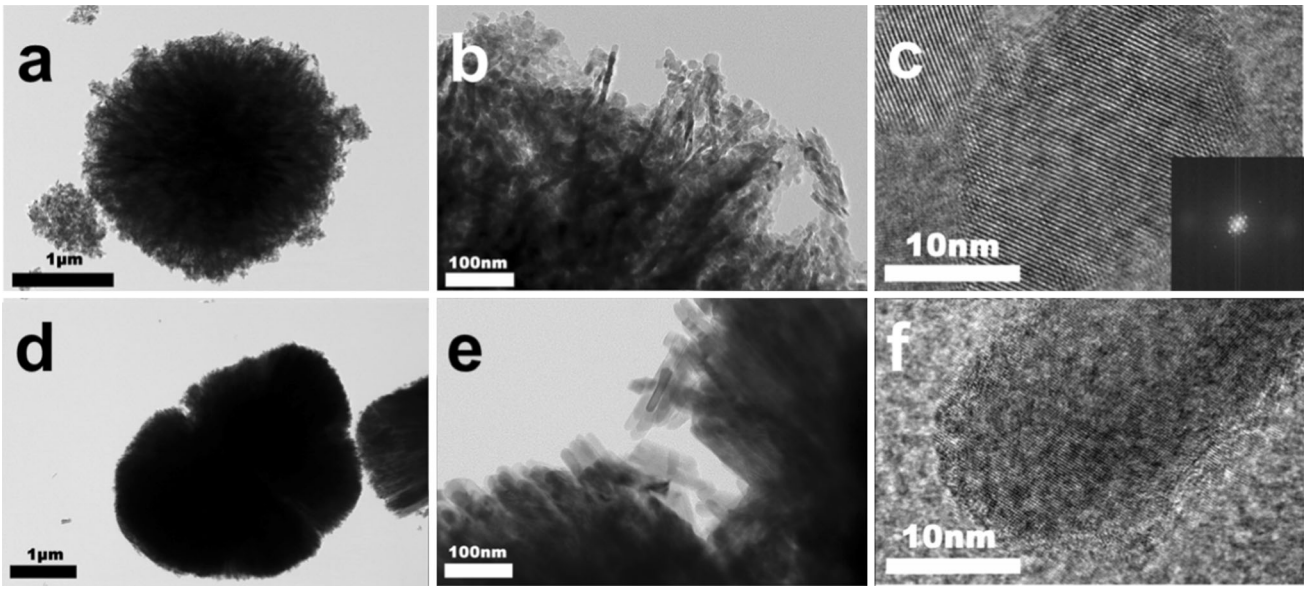

Figure 2 Transmission electron microscopic (TEM) images, DDP pattern and the high-resolution transmission electron microscopic images (HRTEM) of TiO_2 samples **a**–**c** 160 °C; **d**–**f** 190 °C.

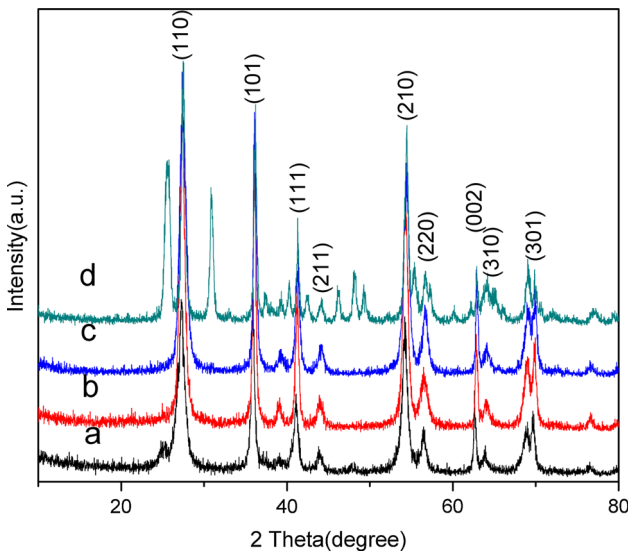

Figure 3 XRD patterns of samples synthesized at 160 °C (**a**), 170 °C (**b**), 180 °C (**c**) and 190 °C (**d**).

where λ is the X-ray wavelength; β is the full width at the half maximum (FWHM) intensity of the diffraction peak; θ is the incident angle; and k is a constant equal to 0.89.

The crystalline dimensions of all the samples are presented in Table 1, which is in good agreement with the TEM observation. Meanwhile, we can calculate that the crystalline sizes of S_{160}, S_{170} and S_{180} are similar, but that of S_{190} is bigger than that of others.

Crystallographic structure of the as-prepared samples judged by Raman spectroscopy shown in Fig. 4 displays that the Raman bands at 609.9, 445, 143.4 and 233.2 cm^{-1} are attributed to the A_{1g}, E_g, B_{1g}, and a second-order phonon mode of rutile phase of TiO_2 [35], respectively. No other bands are observed besides the characteristic bands of rutile TiO_2 in the Raman spectrum of S_{160}, S_{170} and S_{180}. However, new Raman peaks at 323.9 and 366.4 cm^{-1} ascribed to B_{1g} and B_{2g} modes are observed (Fig. 2d), which is characteristic of brookite TiO_2. The results mentioned are well consistent with the above XRD result.

Growth mechanism

In order to find out the role of HCl to the formation of TiO_2 nanostructure, a series of contrast experiments were conducted. As seen in Fig S1 (referred to the supplement data), when HCl was changed to other kinds of acid, such as HNO_3, H_2SO_4, H_3PO_4 and CH_3COOH, distinct bulk structures were achieved even under the same amount of H^+. Therefore, the formation of nanorods can be ascribed to the Cl^- from HCl, which could affect the coordination structure of the growth unit. It is supposed that Cl^- can be selectively adsorbed on the (110) facet of rutile TiO_2 during TBOT hydrolysis, the growth in (110) direction is suppressed, and thus, the TiO_2 particles grow along with the (001) direction [27]. Besides,

Table 1 The crystalline dimensions of all samples

Samples	FWHM (°)	2θ (°)	Crystallite size (nm)	$a = b$ (Å)	c (Å)
S_{160}	0.665	27.28	12.15	4.4582	2.9606
S_{170}	0.620	27.34	13.04	4.4959	3.0587
S_{180}	0.765	27.44	10.57	4.4366	2.9506
S_{190}	0.457	27.52	17.70	4.5852	3.0954

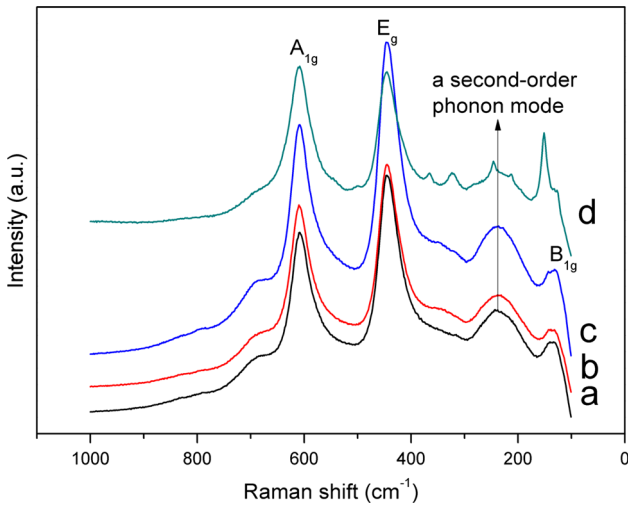

Figure 4 Raman spectra of samples synthesized at 160 °C (**a**), 170 °C (**b**), 180 °C (**c**) and 190 °C (**d**).

XRD patterns of Fig S2 in the supplement data displayed that pure anatase or rutile/anatase mixed crystal structure emerged when the acid was HNO_3, H_2SO_4 or H_3PO_4, indicating that the anion can affect not only the subunit, but also the crystal structure. However, rutile phase still can be obtained along with the increase in the concentration of the HCl (Fig S2e). Therefore, it can be deduced that the coexistence of high acidity and Cl^- prefers to form pure rutile phase, as analyzed before. As for CH_3COOH, faintly acid property leads to the poor crystallinity.

Meanwhile, the influence of the concentration of HCl on the morphology was also studied. When the ratio of HCl/H_2O is about 1/2 (v/v), compact balls were formed at both 160 and 190 °C (Fig S3a and 3c), because the lower concentration of H^+ cannot hinder the hydrolysis rate of TBOT, and the crystallization nucleus grew too fast to be controlled. Though the products are still composed of nanorods, they NRs stacked too compact to obtain a high specific surface area. When the ratio of HCl/H_2O increased to 2/1 (v:v) (Fig S3b and 3d), the TiO_2 nanorods aggregated together and distributed disorderly with no complex nanostructure. Above all, we can conclude that the concentration of HCl is a vital factor to obtain the varied nanostructures.

Furthermore, the mechanism for the formation of hierarchical flower-like TiO_2 nanospheres with rutile phase can be described as follows (Fig. 5). The hydrolysis takes place at lower temperature than 160 °C. Before the temperature reaches 160 °C, the hydrolysis can be completed and structure already exists in similar morphology than that of the final form. Above 160 °C, larger crystallites were obtained due to the crystal growth or recrystallization. At a lower temperature, the amount of crystal nuclei is relatively scarce, leading to form little nanorods. With the temperature elevated, crystal growth effect become more obvious, the size of the subunits decreased and XRD results clearly reveal that the average crystallite size of subunits gradually increased. From 160 to 190 °C, the number of nanorods increases and they can fill up the gaps between clusters. Gradually, the hierarchical flower-like nanospheres are obtained.

BET analysis

The nitrogen adsorption–desorption analysis suggests the porous hierarchy of the TiO_2 materials. All the samples show representative type-IIb(non-reversible type II) curves with H3 hysteresis loops (Fig. 6). These isotherms are characteristic of aggregated powders with slit-shaped pores, and similar isotherms with H3 hysteresis loop were obtained in studies previously [36, 37]. Samples of S_{160}, S_{170}, S_{180} show capillary condensation steps at a little lower relative pressure of 0.4–0.5, suggesting a narrow pore size distribution, which can be confirmed by the pore size distribution inset the isotherm curves. However, the capillary condensation of sample S_{190} postpones to a higher relative pressure of 0.7–0.8, distinctively different from the other three samples. The corresponding pore size distribution curve exhibits a wider pore size distribution, and it has two peak pore diameters of about 3 and 35 nm, while the pore size

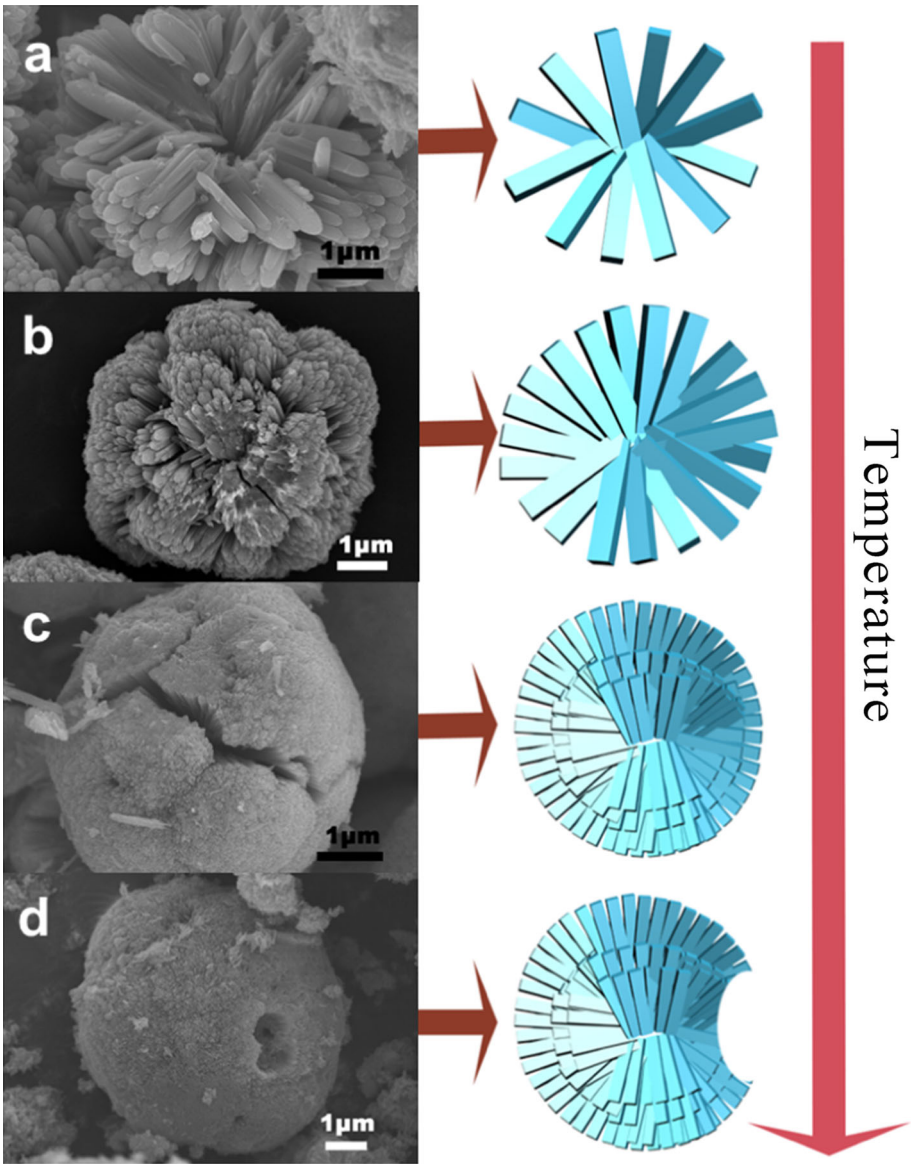

Figure 5 SEM images of hierarchical TiO_2 nanostructures synthesized at different temperatures: **a** 160 °C; **b** 170 °C; **c** 180 °C; **d** 190 °C. The corresponding schematic diagram represents the formation mechanism.

of other three samples is all around 2.6 nm. It is universally acknowledged that the type H3 hysteresis loop is associated with slit-like pores formed by the aggregations of the plate-like particles. Besides, the isotherms show high adsorption at high relative pressure (P/P_0) range (approaching 1.0), indicating the formation of large mesopores and macropores, as analyzed above.

The BET surface area, total pore volume and average pore size of the materials are listed in Table 2. It is found that all the samples have relatively low specific surface areas, calculated by the Brunauer–Emmett–Teller (BET) method. The existence of large mesopores of S_{190} gives rise to a higher surface area.

Photocatalytic activity

Photocatalytic performance of the hierarchical TiO_2 synthesized at various temperatures was tested via the degradation of a complex dye solution containing 10 mg/l RhB and 10 mg/l MB under ultraviolet irradiation. As shown in Fig. 7, the photocatalytic activities of the catalysts showed stronger degradation ability for RhB than for MB. It was found that the S_{160} and S_{190} presented the highest photocatalytic activity. As to S_{160}, nearly 35% RhB and 27% MB were degraded after degradation of 10 min. Furthermore, 90% RhB and 73% MB were absorbed after 60 min of irradiation. The S_{190} exhibited almost equal catalytic activity compared to the S_{160}, but it showed a better

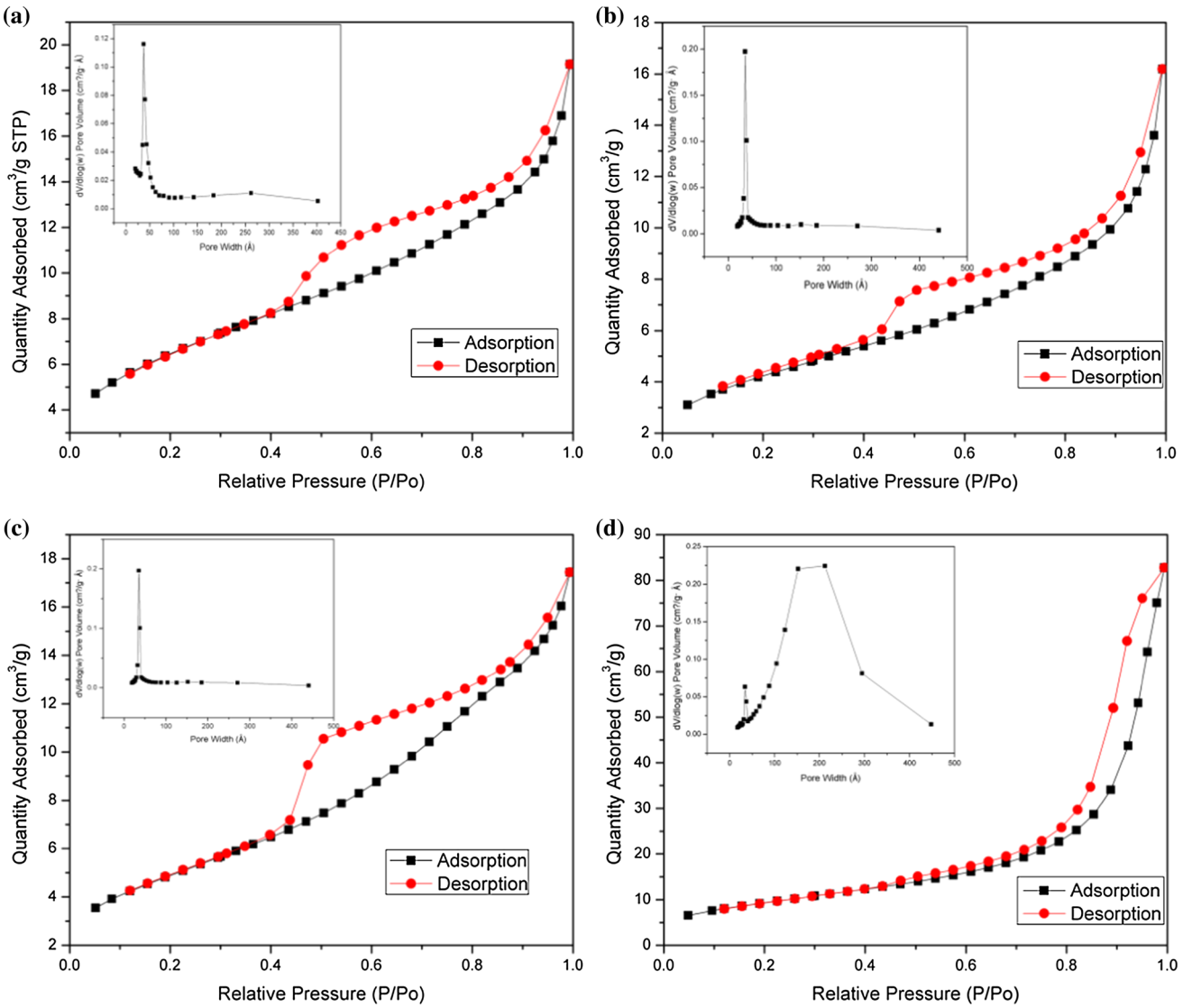

Figure 6 Nitrogen isotherm adsorption–desorption curves of sample S_{160} (**a**), S_{170} (**b**), S_{180} (**c**) and S_{190} (**d**). The *insets* show their pore size distributions.

Table 2 BET surface area, total pore volume and average pore size of the materials

Samples	S_{BET} (m^2g^{-1})	Pore volume (cm^3g^{-1})	Average pore size (nm)	Crystallite size (nm)
S_{160}	23	0.029	5.13	12.15
S_{170}	15	0.025	6.86	13.04
S_{180}	18	0.027	5.67	10.57
S_{190}	34	0.127	13.85	17.70

ability to eliminate MB and the opposite performance to RhB than the S_{160}, with 80% MB and 84% RhB absorbed within 60 min. It can be concluded that the photocatalytic performance follows neither the order of the crystallite size nor the order of specific surface area. The result lies in the synergistic effect of various coexisting factors, especially the high harvesting and good transferring properties of 3D hierarchical flower-like TiO_2 nanostructure. The high photoactivity of S_{160} can be ascribed to the existence of exposed (110) facet [19]. Potentially, the rutile (110) facet offers the reduction sites. The excited holes are more likely to stay at Ti–O–Ti bridging sites rather than at the edge-shared oxygen under irradiation,

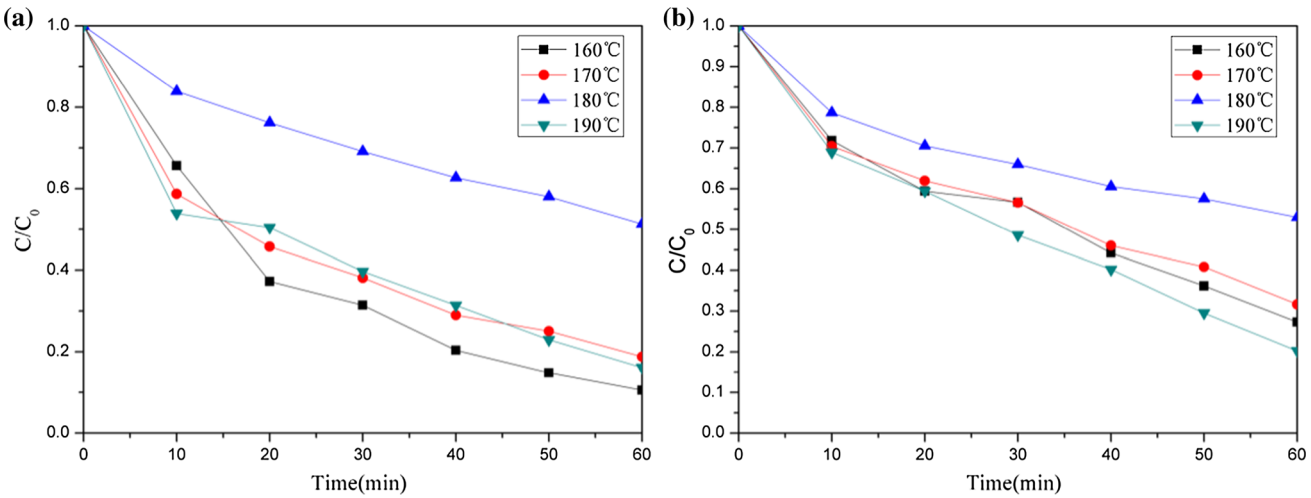

Figure 7 Photocatalytic degradation of RhB and MB simultaneously under UV light irradiation: **a** RhB at 665 nm; **b** MB at 550 nm.

which leads to the weakening of the Ti–O bond and the formation of oxygen defect. It is common sense that the rutile (001) facet involves only edge-shared oxygen atoms and both types of atoms are present in (110) plane. Moreover, titanium atoms on the rutile (110) facet prefer the adsorption of the dissolved oxygen molecules. Therefore, samples containing exposed (110) facet turn out to be more robust catalysts.

BET surface area plays a significant role when the reaction sites were (001) facet. The presence of the sunken hole, large mesopores and macropores increases the BET surface area of S_{190} and subsequently increases the number of active sites. However, the existence of brookite prevents further improvement of the efficiency. Therefore, S_{170} which also contained the exposed (110) facets performed much better than S_{180}, to which almost 53% MB and 51% RhB still remained even after 60 min of irradiation, owning to the lower BET surface area.

Conclusion

In summary, hierarchical flower-like TiO_2 nanospheres with rutile phase were synthesized successfully via a facile one-step and cost-effective hydrothermal method. The architectures were assembled from highly ordered nanorods and turned into 3D dendrites with the increase in reaction temperature, suggesting that the morphology of rutile TiO_2 can be tuned conveniently. Besides, the results show that the high acidity prefers to form rutile phase, and the selective adsorption of Cl^- affects the growth direction of the TiO_2 nanoparticles. Moreover, the photocatalytic degradation of a complex dye solution containing RhB and MB revealed that S_{160} can work as efficient as S_{190} because of the exposed (110) facet though the BET surface area of S_{160} is much smaller. Above all, the complex structured TiO_2 with rutile phase can be tailored easily and it is expected to be promising for the practical use in cleaning up the environment.

Acknowledgements

This work was financially supported by the Shanghai Rising-Star Program (B-type) (15QB1402300), the Minhang District Leading Talent Project (No. 201541), the Shanghai Talent Development Project (No. 201531), Science and technology project Supported by Minhang Government Funds (2016MH195), Natural of science Foundation of Shanghai (17ZR1420000).

Electronic supplementary material: The online version of this article (doi:10.1007/s10853-017-1498-3) contains supplementary material, which is available to authorized users.

References

[1] Fujishima A, Honda K (1972) Electrochemical photolysis of water at a semiconductor electrode. Nature 238:37–38

[2] Ohno T, Tsubota T, Nishijima K, Miyamoto Z (2004) Degradation of methylene blue on carbonate species-doped TiO_2 photocatalysts under visible light. Chem Lett 33:750–751

[3] Ohko Y, Ando I, Niwa C, Tatsuma T (2001) Degradation of bisphenol A in water by TiO_2 photocatalyst. Environ Sci Technol 35:2365–2368

[4] Montoya JF, Atitar MF, Bahnemann DW (2014) Comprehensive kinetic and mechanistic analysis of TiO_2 photocatalytic reactions according to the direct–indirect model: (ii) experimental validation. J Phys Chem C 118:14276–14290

[5] Zhu YX, Wang YF, Chen Z et al (2015) Visible light induced photocatalysis on CdS quantum dots decorated TiO_2 nanotube arrays. Appl Catal A Gen 498:159–166

[6] Soltani RDC, Jorf S, Ramezani H, Purfadakari S (2016) Ultrasonically induced ZnO–biosilica nanocomposite for degradation of a textile dye in aqueous phase. Ultrason Sonochem 28:69–78

[7] Liu JM, Zhang QC, Yang JC, Ma HY, Tade MO, Wang SB, Liu J (2014) Facile synthesis of carbon-doped mesoporous anatase TiO_2 for the enhanced visible-light driven photocatalysis. Chem Commun 50:13971–13974

[8] Hsieh SH, Chen WJ, Wu CT (2015) Pt-TiO_2/graphene photocatalysts for degradation of AO7 dye under visible light. Appl Surf Sci 340:9–17

[9] Chen XB, Liu L, Yu PY, Mao SS (2011) Increasing solar absorption for photocatalysis with black hydrogenated titanium dioxide nanocrystals. Science 331:746–750

[10] Varghese OK, Paulose M, Grimes CA (2009) Long vertically aligned titania nanotubes on transparent conducting oxide for highly efficient solar cells. Nat Nano Technol 4:592–597

[11] Hamid MG, Saif MHQ, Mahmoud H, Joselito PL, Mohammad A, Idriss MB, Abdullah SA (2016) Laser induced photocurrent and photovoltage transient measurements of dye-sensitized solar cells based on TiO_2 nanosheets and TiO_2 nanoparticles. Electrochim Acta 212:992–997

[12] Wang F, Ma ZZ, Ban PP, Xu XH (2017) N and S codoped rutile TiO_2 nanorods for enhanced visible-light photocatalytic activity. Mater Lett 195:143–146

[13] Yang QQ, Peng P, Xiang ZH (2017) Covalent organic polymer modified TiO_2 nanosheets as highly efficient photocatalysts for hydrogen generation. Chem Eng Sci 162:33–40

[14] Lee HU, Lee SC, Lee SM, Lee JW, Kim HJ, Lee J (2013) Improved photocatalytic and antibacterial activities of three-dimensional polycrystalline anatase TiO_2 photocatalysts. Appl Catal A Gen 467:394–399

[15] Xu F, Zhang XY, Wu Y, Wu DP, Gao ZY, Jiang K (2013) Facile synthesis of TiO_2 hierarchical microspheres assembled by ultrathin nanosheets for dye-sensitized solar cells. J Alloys Compd 574:227–232

[16] Bai HW, Liu ZY, Lee SS, Sun DD (2012) The effect of fabrication method of hierarchical 3D TiO_2 nanorod spheres on photocatalytic pollutants degradation. Appl Catal A Gen 447:193–199

[17] Tao YG, Xu YQ, Pan J, Gu H, Qin CY, Zhou P (2012) Glycine assisted synthesis of flower-like TiO_2 hierarchical spheres and its application in photocatalysis. Mater Sci Eng B 177:1664–1671

[18] Liao JY, Lei BX, Kuang DB, Su CY (2011) Tri-functional hierarchical TiO_2 spheres consisting of anatase nanorods and nanoparticles for high efficiency dye-sensitized solar cells. Energy Environ Sci 4:4079–4085

[19] Fang S, Jing S, Lian G (2011) Template-free synthesis of hierarchical TiO_2 structures and their application in dye-sensitized solar cells. ACS Appl Mater Interfaces 3:2148–2153

[20] Wang XL, He HL, Chen Y, Zhao JQ, Zhang XY (2012) Anatase TiO_2 hollow microspheres with exposed 001 facets: facile synthesis and enhanced photocatalysis. Appl Surf Sci 258:5863–5868

[21] Dong YS, Fei XN, Liu ZF, Zhou YZ, Cao LY (2017) Synthesis and photocatalytic redox properties of anatase TiO_2 single crystals. Appl Surf Sci 394:386–393

[22] Yadav Hemraj M, Jung-Sik Kim (2016) Solvothermal synthesis of anatase TiO_2-graphene oxide nanocomposites and their photocatalytic performance. J Alloys Compd 688:123–129

[23] Kobayashi M, Petrykin V, Kakihana M (2009) Hydrothermal synthesis and photocatalytic activity of whisker-like rutile-type titanium dioxide. J Am Ceram Soc 92:S21–S26

[24] Tao T, Chen Y (2013) Direct synthesis of rutile TiO_2 nanorods with improved electrochemical lithium ion storage properties. Mater Lett 98:112–115

[25] Truong QD, Hoa HT, Le TS (2017) Rutile TiO_2 nanocrystals with exposed 331 facets for enhanced photocatalytic CO_2 reduction activity. J Colloid Interface Sci 504:223–229

[26] Han B, Kim SJ, Hwang BM, Kim SB, Park KW (2013) Single-crystalline rutile TiO_2 nanowires for improved lithium ion intercalation properties. J Power Sources 222:225–229

[27] Sun B, Zhou GW, Zhang Y, Liu RR, Li TD (2015) Photocatalytic properties of exposed crystal surface-controlled rutile TiO_2 nanorod assembled microspheres. Chem Eng J 264:125–133

[28] Yurdakal S, Palmisano G, Loddo V, Augugliaro V, Palmisano L (2008) Nanostructured rutile TiO_2 for selective photocatalytic oxidation of aromatic alcohols to aldehydes in water. J Am Chem Soc 130:1568–1569

[29] Ohno T, Tsubota T, Toyofuku M, Inaba R (2004) Photocatalytic activity of a TiO_2 photocatalyst doped with C^{4+} and S^{4+} ions having a rutile phase under visible light. Catal Lett 98:255–258

[30] Lin J, Yu JC, Lo D, Lam SK (1999) Photocatalytic activity of rutile $Ti_{1-x}Sn_xO_2$ solid solutions. J Catal 183:368–372

[31] Ramanathan R, Bansal V (2015) Ionic liquid mediated synthesis of nitrogen, carbon and fluorine-codoped rutile TiO_2 nanorods for improved UV and visible light photocatalysis. RSC Adv 5:1424–1429

[32] Yan C, Feng DJ, Jiang YJ, An XY, Ye LJ, Guan WS, Bai B (2015) Bio-template route for the facile fabrication of TiO_2@bacillus subtilis composite particles and their application for the degradation of rhodamine B. Catal Lett 145:1301–1306

[33] Du SN, Liao ZJ, Qin ZL, Zuo F, Li XH (2015) Polydopamine microparticles as redox mediators for catalytic reduction of methylene blue and rhodamine B. Catal Commun 72:86–90

[34] Yang J, Mei S, Ferreira JMF (2000) Hydrothermal synthesis of nanosized titania powders: influence of peptization and peptizing agents on the crystalline phases and phase transitions. J Am Ceram Soc 83:1361–1368

[35] Cheng HM, Ma JM, Zhao ZG, Qi LM (1995) Hydrothermal preparation of uniform nanosize rutile and anatase particles. Chem Mater 7:663–671

[36] Kőrösi L, Prato M, Scarpellini A, Kovács J, Dömötör D, Kovács T, Papp S (2016) H_2O_2-assisted photocatalysis on flower-like rutile TiO_2 nanostructures: rapid dye degradation and inactivation of bacteria. Appl Surf Sci 365:171–179

[37] Kőrösi L, Papp S, Oszkó A, Dékány I (2012) Low-temperature sintering behavior of nanocrystalline indium tin oxide prepared from polymer-containing sols. Mater Res Bull 47:933–940